

Label-free multimodal nonlinear optical microscopy reveals fundamental insights of skeletal muscle development

Qiqi Sun,^{1,4} Yanfeng Li,^{2,4} Sicong He,¹ Chenghao Situ,²
Zhenguo Wu,^{2,3} and Jianan Y. Qu^{1,3,*}

¹Department of Electronic and Computer Engineering, Hong Kong University of Science and Technology, Clear Water Bay, Kowloon, Hong Kong SAR, China

²Division of Life Science, Hong Kong University of Science and Technology, Clear Water Bay, Kowloon, Hong Kong SAR, China

³Center of Systems Biology and Human Health, School of Science and Institute for Advanced Study, Hong Kong University of Science and Technology, Clear Water Bay, Kowloon, Hong Kong SAR, China

⁴These authors contributed equally to this work

*eequ@ust.hk

Abstract: We developed a label-free nonlinear optical (NLO) microscope integrating the stimulated Raman scattering, multi-color two-photon excited fluorescence and second harmonic generation. The system produces multimodal images of protein content, mitochondria distribution and sarcomere structure of fresh muscle samples. With the advanced imaging technique, we studied the mal-development of skeletal muscle caused by sarcomeric gene deficiency. In addition, important development processes of normal muscle from neonatal to adult stage were also clearly revealed based on the changing sarcomere structure, mitochondria distribution and muscle fiber size. The results demonstrate that the newly developed multimodal NLO microscope is a powerful tool to assess the muscle integrity and function.

©2013 Optical Society of America

OCIS codes: (170.3880) Medical and biological imaging; (170.6930) Tissue; (180.4315) Nonlinear microscopy; (290.5910) Scattering, stimulated Raman

References and links

1. K. K. Griendling, J. A. Hill, and E. N. Olson, *Muscle: fundamental biology and mechanisms of disease* (Elsevier Science, 2012).
2. K. Schuster-Gossler, R. Cordes, and A. Gossler, "Premature myogenic differentiation and depletion of progenitor cells cause severe muscle hypotrophy in Delta1 mutants," *Proc. Natl. Acad. Sci. U.S.A.* **104**(2), 537–542 (2007).
3. R. T. Dirksen, "Sarcoplasmic reticulum-mitochondrial through-space coupling in skeletal muscle," *Appl. Physiol. Nutr. Metab.* **34**(3), 389–395 (2009).
4. S. V. Plotnikov, A. M. Kenny, S. J. Walsh, B. Zubrowski, C. Joseph, V. L. Scranton, G. A. Kuchel, D. Dauser, M. Xu, C. C. Pilbeam, D. J. Adams, R. P. Dougherty, P. J. Campagnola, and W. A. Mohler, "Measurement of muscle disease by quantitative second-harmonic generation imaging," *J. Biomed. Opt.* **13**(4), 044018 (2008).
5. R. F. E. Crang and K. L. Klomparens, *Artifacts in biological electron microscopy* (Plenum Press, 1988).
6. H. Chen, H. Wang, M. N. Slipchenko, Y. Jung, Y. Shi, J. Zhu, K. K. Buhman, and J. X. Cheng, "A multimodal platform for nonlinear optical microscopy and microspectroscopy," *Opt. Express* **17**(3), 1282–1290 (2009).
7. J. Lin, F. Lu, W. Zheng, S. Xu, D. Tai, H. Yu, and Z. Huang, "Assessment of liver steatosis and fibrosis in rats using integrated coherent anti-Stokes Raman scattering and multiphoton imaging technique," *J. Biomed. Opt.* **16**(11), 116024 (2011).
8. S. V. Plotnikov, A. C. Millard, P. J. Campagnola, and W. A. Mohler, "Characterization of the myosin-based source for second-harmonic generation from muscle sarcomeres," *Biophys. J.* **90**(2), 693–703 (2006).
9. D. Li, W. Zheng, and J. Y. Qu, "Imaging of epithelial tissue *in vivo* based on excitation of multiple endogenous nonlinear optical signals," *Opt. Lett.* **34**(18), 2853–2855 (2009).
10. P. B. Conibear, A. Málnási-Csizmadia, and C. R. Bagshaw, "The effect of F-actin on the relay helix position of myosin II, as revealed by tryptophan fluorescence, and its implications for mechanochemical coupling," *Biochemistry* **43**(49), 15404–15417 (2004).

11. C. P. Pfeffer, B. R. Olsen, F. Ganikhanov, and F. Légaré, "Imaging skeletal muscle using second harmonic generation and coherent anti-Stokes Raman scattering microscopy," *Biomed. Opt. Express* **2**(5), 1366–1376 (2011).
12. C. Brackmann, B. Gabrielsson, F. Svedberg, A. Holmaang, A. S. Sandberg, and A. Enejder, "Nonlinear microscopy of lipid storage and fibrosis in muscle and liver tissues of mice fed high-fat diets," *J. Biomed. Opt.* **15**(6), 066008 (2010).
13. C. W. Freudiger, W. Min, B. G. Saar, S. Lu, G. R. Holtom, C. He, J. C. Tsai, J. X. Kang, and X. S. Xie, "Label-free biomedical imaging with high sensitivity by stimulated Raman scattering microscopy," *Science* **322**(5909), 1857–1861 (2008).
14. D. Fu, G. Holtom, C. Freudiger, X. Zhang, and X. S. Xie, "Hyperspectral imaging with stimulated Raman scattering by chirped femtosecond lasers," *J. Phys. Chem. B* **117**(16), 4634–4640 (2013).
15. E. C. Rothstein, S. Carroll, C. A. Combs, P. D. Jobsis, and R. S. Balaban, "Skeletal muscle NAD(P)H two-photon fluorescence microscopy *in vivo*: topology and optical inner filters," *Biophys. J.* **88**(3), 2165–2176 (2005).
16. P. Rochard, A. Rodier, F. Casas, I. Cassar-Malek, S. Marchal-Victorion, L. Dauray, C. Wrutniak, and G. Cabello, "Mitochondrial activity is involved in the regulation of myoblast differentiation through myogenin expression and activity of myogenic factors," *J. Biol. Chem.* **275**(4), 2733–2744 (2000).
17. D. Frank, C. Kuhn, H. A. Katus, and N. Frey, "The sarcomeric Z-disc: a nodal point in signalling and disease," *J. Mol. Med.* **84**(6), 446–468 (2006).
18. I. Dalkilic, J. Schienda, T. G. Thompson, and L. M. Kunkel, "Loss of FilaminC (FLNc) results in severe defects in myogenesis and myotube structure," *Mol. Cell. Biol.* **26**(17), 6522–6534 (2006).
19. Q. Zhou, P. H. Chu, C. Huang, C. F. Cheng, M. E. Martone, G. Knoll, G. D. Shelton, S. Evans, and J. Chen, "Ablation of Cypher, a PDZ-LIM domain Z-line protein, causes a severe form of congenital myopathy," *J. Cell Biol.* **155**(4), 605–612 (2001).
20. V. Dubowitz, "Enzyme histochemistry of skeletal muscle," *J. Neurol. Neurosurg. Psychiatry* **28**(6), 516–524 (1965).

1. Introduction

Muscle is the most abundant tissue in human and most of other animal species. Skeletal muscle, a type of striated muscle, is attached to bones and responsible for the voluntary body movement [1]. The skeletal muscle cells/fibers are developed from muscle precursors in the myotome at the embryonic stage. After cell fate determination, the cells will undergo differentiation and fuse to form multi-nucleated myotubes. During myotube formation, the sarcomeres, the basic structure responsible for muscle movement, are formed [2]. Even after birth, the sarcomeres are not fully formed and still need several months to mature [3]. Any abnormal development caused by gene deficiency or secondarily associated with the onset of other diseases such as cachexia, atrophy, or sarcopenia could lead to muscular disorders and other severe diseases [2,4]. A variety of imaging technologies with their own advantages and disadvantages have been used to study the muscle development processes. The conventional bright-field microscopy requires exogenous markers to image specific parts of muscle and does not have depth resolved imaging capability. Confocal microscopy is difficult to achieve label-free multimodal imaging, a desirable function in the study of complex biological mechanisms and systems. Furthermore, the short penetration depth limits its application at tissue level. For high resolution electron microscopy, the multiple-step preparation procedures of biological samples frequently cause alteration of tissue structure and loss of information [5]. Previously, label-free imaging of living cells, fresh spinal tissue and liver were achieved by multimodal nonlinear optical (NLO) microscopy integrating coherent anti-Stokes Raman scattering (CARS), second/third harmonic generation (SHG/THG) and two-photon excited fluorescence (TPEF) [6,7]. In this work, we develop a multimodal NLO microscope to study the skeletal muscle development in a mice model. This label-free imaging technique examines freshly isolated muscle tissue and minimizes the sample preparation that causes possible alteration of tissue morphology.

The multi-nucleated muscle fibers are abundant of endogenous signal sources for NLO microscopy. Myosin, a major contractile sarcomeric protein responsible for muscle movement, can produce SHG for quantitative characterization of sarcomere disorders in the muscle fibers [4,8]. Tryptophan, one of the amino acids, is another endogenous fluorophore in proteins. The tryptophan fluorescence can convey the information of protein content and reveal cellular morphology [9]. Also, tryptophan fluorescence was used to study the interaction between actin and myosin, the sarcomeric proteins [10]. Coherent Raman

scattering microscopy is another label-free technology to image proteins in biological samples. CARS microscopy had shown the capability to image the sarcomeric sub-structure in fixed skeletal muscle sample [11]. With appropriate frequency difference of two laser beams, CARS microscopy can also image the lipid storage in the muscle tissue [12]. Compared to the CARS, the stimulated Raman scattering (SRS) microscopy can image the protein and lipid without nonresonant background [13,14]. The reduced nicotinamide adenine dinucleotide (NADH), an indicator of cell metabolism, is one of most frequently used endogenous fluorophore for label-free imaging of mitochondria in biological cells [9]. In the mature skeletal muscle fibers, mitochondria can be grouped into the category of perivascular, paranuclear, subsarcolemmal and intersarcomeric, in which intersarcomeric mitochondria are orderly arranged in the muscle fibers and correlate with calcium signaling [3,15]. Mitochondria not only provide ATP to muscle cells, but also play an important role in regulating the myoblast differentiation [16].

In this study, we develop a NLO microscope system integrating SRS, TPEF and SHG. The system excites all endogenous NLO signals discussed above and produces the multimodal images of crucial biomorphological information for visualizing the development of skeletal muscle. Specifically, the images collected from freshly isolated muscle samples reveal the lipid and protein distributions, myosin filament integrity, and mitochondria pattern in the muscle fibers. With this technique, we studied the mal-development of skeletal muscle fibers caused by sarcomeric gene mutation and the maturation of skeletal muscle in normal development process.

2. Methods and materials

The schematic of multimodal nonlinear microscope is shown in Fig. 1(a). A Ti:sapphire femtosecond laser with 80MHz repetition rate (Chameleon Ultra II, Coherent) was tuned at 740nm to excite TPEF of NADH and SHG of myosin filament simultaneously. When the laser was tuned at 830nm, 10% output power was used as pump beam of SRS and 90% output power was used to pump an optical parametric oscillator (OPO) (Chameleon OPO, Coherent) to generate an 1100nm femtosecond laser beam. Part of 1100 nm was frequency doubled after passing through a Beta Barium Borate (BBO) crystal to generate a femtosecond laser beam at 550nm for the excitation of tryptophan TPEF signal. The 1100nm laser through BBO was separated from 550nm beam by a dichroic mirror (DM1: 850DCSPXR, Chroma) and was used as the Stokes beam of SRS. The frequency difference between 830nm (pump) and 1100nm (Stokes) matches the $-\text{CH}_3$ bond stretching vibration at 2950cm^{-1} of lipid and proteins [14]. A pair of prisms was introduced to the Stokes beam to compress the pulse duration before the beam passed through a 10.7MHz acousto-optic modulator (3080-122, Crystal Technology). Finally, three laser beams were combined by two dichroic mirrors (DM2: 900DCXXR and DM3: 710DCXR, Chroma) in turn and went through a pair of galvo mirrors (6800H, Cambridge Technology) for x-y lateral scanning. A water immersion objective (UAPON 40XW340, 1.15 NA, Olympus) was driven by an actuator (Z625B, Thorlabs) to achieve the axial section.

Signals were collected in both backward and forward directions. In backward direction, a dichroic mirror (DM4: FF510-Di01, Semrock) reflected the TPEF and weak SHG signals to a spectrograph equipped with a 16 PMT array and a time correlated single photon counting (TCSPC) module (PML-16-C-0 and SPC-150, Becker & Hickl). Two short pass filters (SP01-532RU and SP01-633RS, Semrock) were used to remove the exciting light. The spectrograph detected light of wavelength ranged from 312nm to 507nm with 13nm resolution, which covered the TPEF signals of tryptophan and NADH. Typical NADH and tryptophan TPEF spectra recorded from the fresh skeletal muscle samples are shown in Fig. 1(b). In forward direction, the signals were collected by a condenser (U-AAC, Achromat/aplanat condenser, NA 1.4, Olympus) and the SRS and SHG of 740nm were separated by a dichroic mirror (DM5: 760dcxr, Chroma). The strong forward SHG signal was further selected by two filters (Fs2: FF01-357/44, FF01-680/SP, Semrock) and recorded by a single channel PMT (H10682-210, Hamamatsu); the SRS signal beam (pump beam at 830 nm) was selected out

by other pair of filters (Fs1: FF01-794/160, Semrock and 64335 shortpass 900 nm, Edmund) and recorded by a photodiode (FDS 100, Thorlabs). The SRS signal was demodulated by a high-frequency lock-in amplifier (SR844, Stanford Research Systems). Overall, the excitation power (before the objective) of 550nm, 740nm, 830nm and 1100nm beams was about 6mW, 30mW, 25mW and 30mW, respectively. All the images were formed with 256×256 pixels over $100\mu\text{m} \times 100\mu\text{m}$ field of view and the integration time was less than 16s. All the tissue samples were oriented carefully to make muscle fibers elongate in the diagonal direction (see Figs. 2 and 3). This maximized the SHG intensity because the angle of myosin filament and laser beam polarization was roughly set to 45° in this study though similar results can be obtained by using the excitation of different polarization [8].

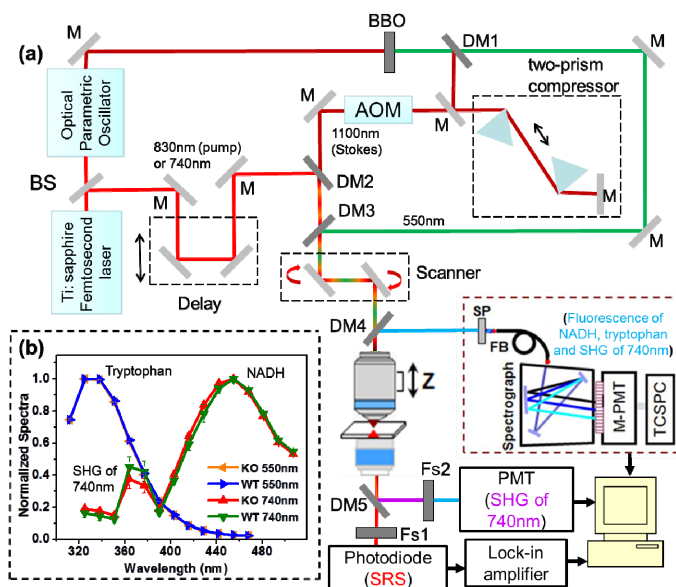


Fig. 1. (a) Schematic of the multimodal nonlinear microscope. M: mirror; BS: beam splitter; DM: dichroic mirror; BBO: Beta Barium Borate crystal; AOM: acousto-optic modulator; SP: short pass filter; Fs: filter set; M-PMT: 16 channels photomultiplier. (b) Normalized TPEF and SHG spectra of TA muscle from KO and WT neonatal mice under 550nm and 740nm excitation.

The C57BL/6J mice model was used in the study. In details, we firstly conducted a study to reveal how the skeletal muscle developments are determined by the genes possibly related to the assembly of sarcomere [17–19]. The tibialis anterior (TA) muscles with bone attached were freshly isolated from the wild type (WT) and gene knocked out (KO) neonatal and 17-day embryonic mice. The TA muscles were soaked in phosphate buffered saline (PBS) and directly imaged by the NLO microscope. Secondly, we study the muscle normal development from neonatal to adult stage. The TA muscles were freshly isolated from 3-week and 5-month old WT mice and soaked in PBS during imaging by the NLO microscope. The thickness of TA muscle samples from the new born mice was approximately 0.5mm and the thickness of TA muscle samples from adult mice was approximately 1 to 1.5mm. All images were taken within two hours after the muscle isolation and all studies were approved by the Animal Ethics Committee of Hong Kong University of Science and Technology.

3. Results and discussions

To study the mal-development of skeletal muscle fibers caused by sarcomeric gene mutation, we examined the TA muscles isolated from the wild type (WT) and gene knocked out (KO) neonatal mice. The multimodal images are shown in Fig. 2. In details, the SRS, tryptophan TPEF (312-370nm), forward SHG and NADH TPEF (416-507nm) images of WT and KO

mice TA muscles are displayed from top to bottom in column (a) and (b), respectively. As shown in Figs. 2(a1)-(a2) and 2(b1)-(b2), the SRS and tryptophan TPEF images provide information of the basic structures of muscle fibers. Though tryptophan TPEF signal can only be excited from the proteins with the fluorescent amino acid and SRS signals are not selective for all proteins, we found that most of information in the SRS and tryptophan images are identical. Morphologically, the muscle fibers in WT mice are more in order than the KO mice. The bright spots (marked with arrowhead) in SRS images of WT and KO mice are possibly lipid droplets because all the other image modalities do not show the spots and lipid droplets were also been observed in muscle tissue by CARS microscopy [12]. However, a SRS system of high spectral resolution is required to verify whether the bright spots are truly lipid droplets [7]. In the forward SHG images, clear differences between WT and KO mice muscle can be observed as shown in Figs. 2(a3) and 2(b3). The sarcomeres are densely aligned in order in the normal muscle fibers, while the disrupted sarcomeres are observed in most part of muscle fibers in KO mice. As shown in Figs. 2(a4) and 2(b4), the NADH TPEF images display that in the normal muscle mitochondria are orderly arranged along the sarcomeres, while the cells with relatively chaotic distribution of mitochondria appear in the KO mice muscle tissue. Here, an important finding is that the regions of sarcomere disruption are still filled up with living cells as shown in Figs. 2(b1-2) and 2(b4), indicating that the knocked out gene may mainly affect the sarcomere related development. Moreover, the existence of defective sarcomeres in the KO mice was independently confirmed by electron microscopy study (Li and Wu, unpublished data). We also measured the myosin protein expression level in KO and WT mice muscles and the results showed no difference between KO and WT mice (Li and Wu, unpublished data). This indicated that the extinction of SHG signals in the KO mice muscle is due to that the ordering of the myosin proteins is loosed or lost. Furthermore, we imaged TA muscles of the 17-day embryos of both WT and KO mice. The results displayed in Fig. 2 right column demonstrate that the disruption of sarcomere in KO mice already occurs during embryonic stage. Overall, the normal and abnormal skeletal muscle tissue can be clearly distinguished based on the multimodal images of the information on protein content distribution in cells, myosin filament structure in sarcomere and mitochondria arrangement pattern.

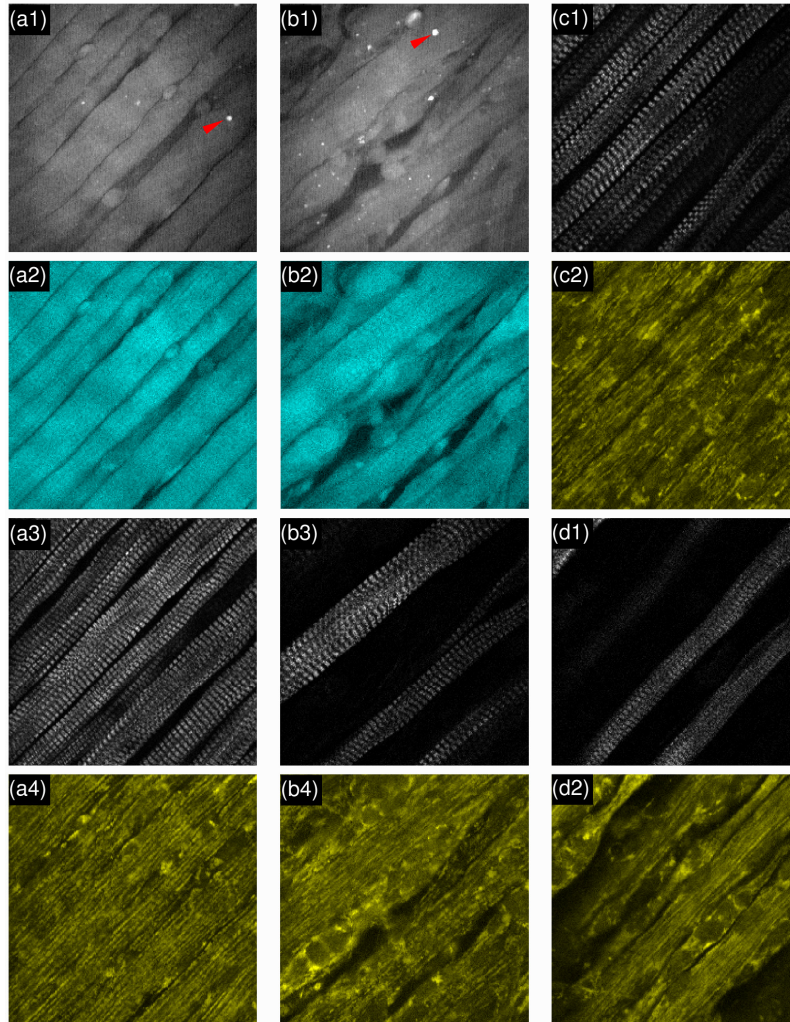


Fig. 2. Multimodal images of neonatal and embryonic mice. (a1)-(a4): SRS, tryptophan TPEF, forward SHG, NADH TPEF images of WT neonatal mice; (b1)-(b4): SRS, tryptophan TPEF, forward SHG, NADH TPEF images of KO neonatal mice; (c1),(c2): Forward SHG, NADH TPEF images of WT 17-day embryonic mice; (d1),(d2): Forward SHG, NADH TPEF images of KO 17-day embryonic mice. Field of view of all images is $100\mu\text{m} \times 100\mu\text{m}$. Arrowhead: bright spot of lipid droplet.

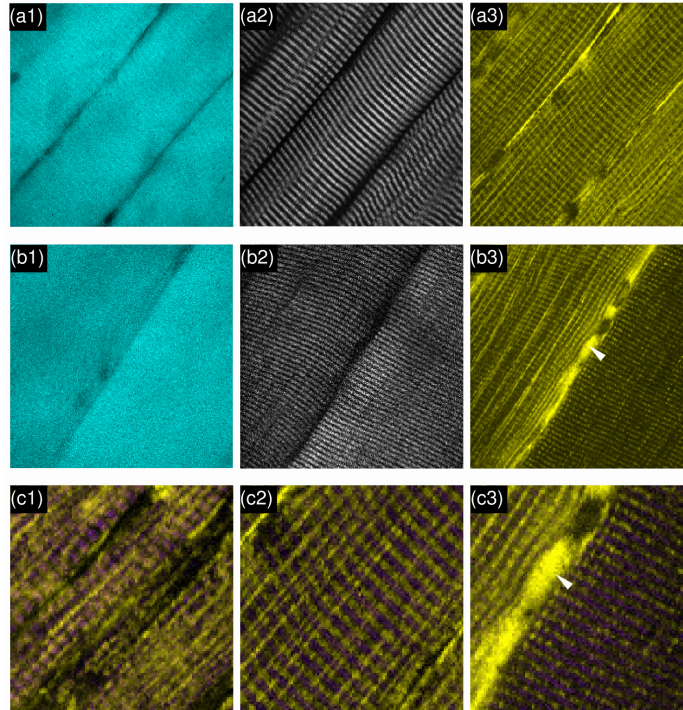


Fig. 3. Multimodal images of 3-week and 5-month old mice. (a1)-(a3): Tryptophan TPEF, forward SHG, NADH TPEF images of 3-week old mice; (b1)-(b3): Tryptophan TPEF, forward SHG, NADH TPEF images of 5-month old mice; (c1)-(c3): Zoomed-in superimposed images of forward SHG (colored as violet) and NADH TPEF (colored as yellow) of WT neonatal, 3-week, 5-month old mice. Field of view of row (a)&(b) is $100\mu\text{m} \times 100\mu\text{m}$ and row (c) is $40\mu\text{m} \times 40\mu\text{m}$. Arrowhead: subsarcolemmal mitochondria.

To study the muscle normal development from neonatal to adult stage, we further examined the TA muscles isolated from 3-week and 5-month old WT mice. Their multimodal images are shown in row (a) and (b) of Fig. 3. Because the SRS provides similar information to tryptophan TPEF signal and it cannot be acquired simultaneously with NADH TPEF signal excited at 740 nm, SRS images was not used in the study of maturation of skeletal muscle. As can be seen from the tryptophan TPEF images in Fig. 2(a2) and Figs. 3(a1) and 3(b1), the muscle fiber size increases significantly as the progress of the maturation. To understand the changes of sarcomere structure and mitochondria distribution in the maturation of muscle, we analyzed the SHG and NADH TPEF images using a 2D Fast Fourier Transform (FFT) method. The 2D spatial frequency spectra of the myosin SHG images of neonatal, 3-week and 5-month old mice are displayed in Figs. 4(a1), 4(b1) and 4(c1), respectively. The harmonic frequency peaks in the spectra clearly indicates the periodic pattern of myosin in sarcomere, and the fundamental frequency (marked with arrowhead) can be used to calculate the sarcomere period length. The calculated sarcomere period lengths of neonatal, 3-week and 5-month old mice are $(2.79 \pm 0.33\mu\text{m})$, $(2.92 \pm 0.12\mu\text{m})$ and $(2.30 \pm 0.07\mu\text{m})$, respectively, which is consistency with previous study in adult mice ($2.34 \pm 0.17\mu\text{m}$ in TA muscle) [15]. The difference in sarcomere period between 5-month old and neonatal/3-week old mice is significant ($p < 0.01$, $n \geq 5$), which could be potentially used as a marker for *in vivo* evaluation of muscle maturation. Next, we analyzed the spatial frequency spectra of NADH TPEF images. As displayed in Figs. 4(a2), 4(b2) and 4(c2), the harmonic frequencies only clearly appear in the images from 3-week and 5-month old mice and the fundamental frequencies (marked with arrowhead) are identical to those found from their corresponding SHG images, meaning that significant amount of mitochondria are distributed in sarcomere by the same period with myosin. However, no obvious harmonic frequency was found in the TA muscle

of neonatal mice, indicating that mitochondria distribution is not correlated to the sarcomere structure. To visualize the quantitative results, we superimposed the SHG and NADH TPEF images and the zoomed-in images display in row (c) of Fig. 3, which confirm that no correlation between mitochondria distribution and myosin pattern in neonatal mice. There is an obvious z-line alignment preference for the mitochondria in the 3-week and 5-month old mice muscle fibers meaning that the myosin and mitochondria appear alternatively along the muscle fiber with the same period or spatial frequency. The results are consistent with the study in *flexor digitorum brevis* muscle aged from 0.5 to 4 months and the change of mitochondria alignment may be caused by sarcoplasmic reticulum-mitochondrial “through-space” coupling mechanism [3].

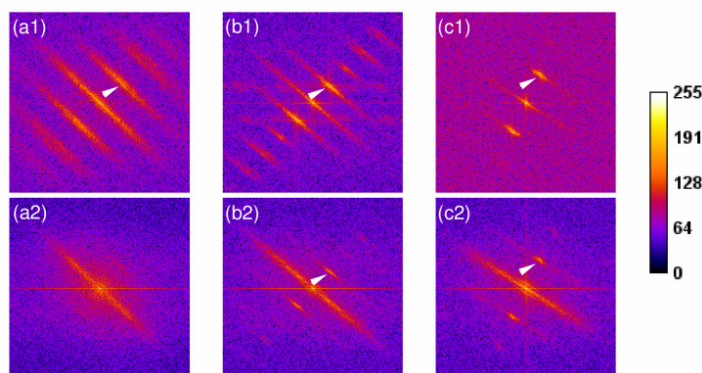


Fig. 4. 2D spatial spectra. Upper row: 2D spectrum of SHG images of WT neonatal (a1), 3-week (b1) and 5-month (c1) old mice. Lower row: 2D spectrum of NADH TPEF images of WT neonatal (a2), 3-week (b2) and 5-month (c2) old mice. The 2D FFT spectral images are generated by ImageJ software. Arrowhead: Fundamental frequency of sarcomere.

Finally, we found that the density of mitochondria in muscles of neonatal and 3-week old mice (Fig. 2(a4) and Fig. 3(a3)) are generally homogenous because the fiber type specification has not occurred in early development stage, which is consistent with previously published result that the enzyme reactions were uniform in all the muscle fibers at early postnatal stage [20]. In contrast, an obvious heterogeneity can be seen in adult mice. Figure 3(b3) displays the NADH TPEF image of two different types of muscle fibers. The fiber on the left side consists of the intersarcomeric mitochondria both precisely aligned with z-line and longitudinally distributed along the sarcomeres, and the subsarcolemmal mitochondrial aggregates (marked with arrowhead). It can be identified as Type IIA/D muscle based on the mitochondria distribution pattern [15]. In the muscle fiber on the right side we only found lower density z-line mitochondria. It can be identified as Type IIB [15]. This indicates that the muscles of 5-month old mice have matured and subdivided into different muscle types.

4. Conclusion

In summary, the multimodal NLO microscope reported in this study provided a quick, reliable and label-free imaging technique for direct visualization of the development of skeletal muscles from different angles. We demonstrated that this method is a powerful tool to study the integrity of skeletal muscle in mutant mice with mutations in sarcomeric genes and to reveal the development process of normal skeletal muscles from neonatal to adult stages. The discovery of sarcomere disruption caused by gene deficiency could contribute to the knowledge of pathophysiological and therapeutical topics related to muscle diseases and treatments. In principle, the structural integrity of the sarcomere in skeletal muscles could be studied using other conventional techniques (e.g., immunostaining, and electron microscopy). However, with those techniques, sample preparations are very tedious and time consuming and the images acquired are prone to artifacts. Our study demonstrated that the label-free multimodal NLO microscope can be used to examine sarcomere integrity and to generate

reliable images with minimal sample manipulation at tissue level. In addition, the multimodal NLO microscope produces multi-modal images simultaneously, making *in vivo* examination of living tissue possible. Our study with fresh tissue have served as a proof of principle that the multimodal NLO microscopy technology can be potentially used for *in vivo* imaging of muscle integrity in living animals. This is the unique advantage of multimodal NLO microscopy over other conventional imaging techniques.

Acknowledgment

This work was supported by the Hong Kong Research Grants Council through grants 662513, 662711, N_HKUST631/11, T13-607/12R, T13-706/11-1, AOE/M-09/12, and Hong Kong University of Science & Technology (HKUST) through grant RPC10EG33.